american physiological society

JNP JOURNAL OF NEUROPHYSIOLOGY

J Neurophysiol 127: 1417–1425, 2022.
First published April 7, 2022; doi:10.1152/jn.00047.2022

RESEARCH ARTICLE

Neural Circuits

Brain temperature affects quantitative features of hippocampal sharp wave ripples

Peter C. Petersen,[1]* Mihály Vöröslakos,[1]* and György Buzsáki[1,2]

Neuroscience Institute, School of Medicine, New York University, New York City, New York and Department of Neurology, School of Medicine, New York University, New York City, New York

Abstract

Biochemical mechanisms are temperature dependent. Brain temperature shows wide variations across brain states, and such changes may explain quantitative changes in network oscillations. Here, we report on the relationship between various hippocampal sharp wave ripple features to brain temperature. Ripple frequency, occurrence rate, and duration correlated with temperature dynamics. By focal manipulation of the brain temperature in the hippocampal CA1 region, we show that ripple frequency can be increased and decreased by local heating and cooling, respectively. Changes of other parameters, such as the rate of sharp wave-ripple complex (SPW-R) and ripple duration were not consistently affected. Our findings suggest that brain temperature in the CA1 region plays a leading role in affecting ripple frequency, whereas other parameters of SPW-Rs may be determined by mechanisms upstream from the CA1 region. These findings illustrate that physiological variations of brain temperature exert important effects on hippocampal circuit operations.

NEW & NOTEWORTHY During physiological conditions, brain temperature fluctuates approximately 3°C between sleep and active waking. Here, we show that features of hippocampal ripples, including the rate of occurrence, peak frequency, and duration are correlated with brain temperature variations. Focal bidirectional manipulation of temperature in the hippocampal CA1 region in awake rodents show that ripple frequency can be altered in the direction expected from the correlational observations, implying that temperature plays a significant role.

hippocampus; sharp wave ripples; temperature; thermal perturbation

INTRODUCTION

Hippocampal-neocortical communication is thought to be essential for different forms of cognitive behaviors, most notable for memory, imagination, and planning (1, 2). A key physiological pattern in this communication during "offline" brain states (3) is the sharp wave-ripple complex (SPW-R; 4). In recent decades, SPW-Rs were the subject of extensive investigation and implicated in a plethora of functions including memory consolidation (5), sleep homeostasis (6), synaptic plasticity (7), and metabolic regulation (8). A particularly interesting debate revolves around the similar versus distinct features of SPW-Rs that occur in the waking resting animal and nonrapid eye movement (nonREM) sleep (9). An attractive feature of SPW-Rs is their time-compressed spike sequences of past waking experience and their potential to affect future behavior (10–13). Although both forward and reverse replays are present during both waking and nonREM sleep, wake and sleep SPW-Rs may have potentially different functions, given that they are embedded in different constellations of network states. In the waking animal, SPW-Rs may serve memory retrieval (9), memory maintenance (14), stabilization of place cells (15), planning of actions and travel paths (12, 16), or a combination of these functions (17, 18). In contrast, SPW-Rs during nonREM sleep may be critical to consolidate long-term memories (19), for homeostatic maintenance (6), and to affect endocrine functions (8).

The macroscopic features of SPW-Rs, such as their incidence, amplitude, duration, and frequency, may also be different in the sleeping and waking animals. The extracellular sharp wave (SPW) is produced by synchronous transmembrane currents in the apical dendrites of CA1 pyramidal cells,

*Peter C. Petersen and Mihály Vöröslakos contributed equally to this work.
Correspondence: G. Buzsáki (Gyorgy.Buzsaki@nyulangone.org).
Submitted 9 February 2022 / Revised 23 March 2022 / Accepted 4 April 2022

which is triggered by the synchronous CA3 inputs targeting the mid-stratum radiatum (20). The CA3 volley also excites CA1 interneurons and their interaction induces a short-lived fast oscillation (the "ripple"; 110–160 Hz) detected in the local field potential (4, 21–23). The ripple frequency is determined mainly by the local interaction of perisomatic interneurons (22) and the synchrony of pyramidal neuron spikes in each ripple wave within the CA1 region (24), but it is not known why ripple frequencies in the waking and sleeping brain are different. One potential explanation is brain temperature. During physiological conditions brain temperature fluctuations range 2.5°C in humans (25) and 3°C in rodents and the strongest determinant of brain temperature is wake-sleep state rather than circadian phase (26). Previous research has already established that neuronal sequences in birds and slow oscillations and sleep spindles in mammals decelerate when temperature decreases (27–36) and that brain temperature regulation may have restorative functions to the brain (26, 37). To test the hypothesis that ripple features can be explained by temperature, we first examined the correlation between fluctuation of brain temperature and various parameters of SPW-Rs. To offer more direct evidence for the importance of brain temperature in regulating ripples, we artificially cooled and warmed local volume of tissue in the dorsal CA1 region. We observed a strong correlation between hippocampal temperature changes and various aspects of SPW-Rs in the sleep-wake cycle and show that local cooling and warming affect ripples.

METHODS

Subjects and Surgery

Rats (adult male Long–Evans, 250–450 g, 3–6 mo old) were kept in a vivarium on a 12-h light/dark cycle and were housed 2 per cage before surgery and individually after it. All experiments were approved by the Institutional Animal Care and Use Committee at New York University Medical Center.

Animals were anesthetized with isoflurane anesthesia and craniotomies were performed under stereotaxic guidance. A custom designed, 3-D printed base (38, Supplemental Fig. S1*A*) was attached to the skull with metabond, serving as a base for the probe implants and protection. A 12 cm by 12 cm sheet of copper mesh (Dexmet Corporation, Wallingford, CT) had been attached to the base with dental cement (Pearson Dental, Sylmar, CA) before surgery, from which a protecting cap was formed later (38). Rats (Supplemental Table S1) were implanted with either silicon probes or tungsten wire triplets (50 μm diameter) to record local field potential (LFP) and spikes from the CA1 pyramidal layer. The tip of the cooling device was implanted at antero-posterior (AP): −2.5 mm, medial-lateral axis (ML): 2.5 mm, and lowered 2.5 mm below the brain surface, after which it was attached to the skull and base. Silicon probes (NeuroNexus, Ann-Arbor, MI and Cambridge Neurotech, Cambridge, UK) were implanted in the dorsal hippocampus [antero-posterior (AP) −3.5 mm from Bregma and 2.5 mm from the midline along the medial-lateral axis (ML)]. Silicon probes were mounted on custom-made microdrives to allow their precise vertical movement after implantation (38). Probes were implanted above the target region by attaching the microdrives to the skull with dental cement. Craniotomies were sealed with sterile wax. Stainless steel screws were implanted above the cerebellum, serving as ground and reference, respectively, for electrophysiological recordings. At the end of electrode and cryoprobe implantation, the copper mesh was folded upward, connected to the ground screw, and painted with dental cement. The mesh acts as a Faraday cage, shielding the recordings from environmental electric noise and muscle artifacts, provides structural stability and keep debris away from the probe implants. After postsurgery recovery, probes were moved gradually in 50-μm to 150-μm steps until they reached the CA1 the pyramidal layer. The pyramidal layer of the CA1 region was identified by physiological markers: increased unit activity, strong θ oscillations, and phase reversal of the sharp-wave ripple oscillations (39).

Peltier Cooling Device

A passively cooled peltier device was attached to a silver wire that conducted cooling to the CA1 region of the hippocampus. The hot side of a peltier device (00301-9X30-10RU2, TE Technology, Inc., Traverse City, MI) was attached to a copper heatsink (5 mm × 5 mm, Enzotech MOS-C10 Forged Copper MOSFET Heatsinks) with heat-conductive adhesive (Arctic Silver Thermal Adhesive, Arctic Silver Inc., Visalia, CA). The heatsink was manually expanded and copper mesh was soldered to it to increase the surface to air ratio (surface area). A 15-mm long silver wire (200 μm diameter, 782000, A-M systems, Sequim, WA) was attached to the cold side of the peltier device with heat conductive adhesive. A 5-mm long polyimide tube (EW-95820-05, Cole-Parmer, Vernon Hills, IL) was attached around the silver wire, sealed, and a temperature sensor (223Fu3122-07U015, Semitec USA Corp., Torrance, CA) was attached to the tube. Silver wire (1 mm) was exposed at the tip of the cooling device (Fig. 4*A*).

Electrophysiological Recordings

Animals were handled daily and accommodated to the experimenter before surgery. After recovery from surgery, the animals were recorded in their home cages and on a set of behavioral mazes. The behavioral sessions typically lasted 40 min, whereas the total recording time ranged from a couple of hours to a full 24-h session.

Sharp Wave Ripple Detection

A single LFP signal was bandpass filtered in the ripple band (80—240 Hz), and ripples were detected with a fixed minimum amplitude of 48 μV and further fulfilling a duration criterion of 20 ms above 18^2 μV. Ripple events with a duration >150 ms were excluded to minimize artifacts. The detected events were further manually inspected using NeuroScope2 (40), and noise artifacts and false detected events were removed, typically occurring due to electrical artifacts or scratching artifacts. When possible, a reference channel outside the CA1 was also used to filter out false positive ripple events. The channel used for the ripple detection was visually defined from individual ripples, where the ripple power was deemed highest.

Sharp Wave Ripple Metrics

The ripple peak was defined by the most negative peak of the filtered ripple. The ripple duration was determined by the lowest threshold (18 μV). The ripple rate was calculated within

brain states in 30-s wide bins. The ripple peak frequency was determined from the filtered LFP signal in the ripple frequency band (110–180 Hz), and translated into phase by the Hilbert transform. The frequency at the ripple peak was then determined as the instantaneous change in the phase divided by the sample duration (with a Gaussian neighbor event smoothing; SD = 80 events).

Brain Temperature

Brain temperature was measured using either a thermistor or a thermocouple type *k* and recorded using the Intan system analog amplifier at 20 kHz. Temperature data were downsampled first to 1,250 Hz and to 1 Hz for a subset of the analysis.

Brain State Scoring

Brain state scoring was performed as described in the study by Watson et al. (41). In short, spectrograms were constructed with a 1-s sliding 10-s window fast Fourier transform of 1,250 Hz data at log-spaced frequencies between 1 Hz and 100 Hz. Three types of signals were used to score states: broadband LFP, narrowband θ frequency LFP and electromyogram (EMG). For broadband LFP signal, principal component analysis was applied to the *Z*-transformed (1–100 Hz) spectrogram. The first principal component in all cases was based on power in the low (32 Hz) frequencies. θ Dominance was taken to be the ratio of the power at 5–10 Hz and 2–16 Hz from the spectrogram. EMG was extracted from the intracranially recorded signals by detecting the zero time lag correlation coefficients (*r*) between 300 and 600 Hz filtered signals (using a Butterworth filter at 300–600 Hz with filter shoulders spanning to 275–625 Hz) recorded at all sites. Next all states were inspected and curated manually, and corrections were made when discrepancies between automated scoring and user assessment occurred.

QUANTIFICATION AND STATISTICAL ANALYSIS

Electrophysiological recordings were conducted using an Intan recording system: RHD2000 interface board with Intan 64 channel preamplifiers sampled at 20 kHz (Intan Technologies, Los Angeles, CA). See Table 1 for key resources.

Statistical Analyses

All statistical analyses were performed with MATLAB functions or custom-made scripts. For rank order calculation, the probability of participation and firing rate correlations, the unit of analysis was single cells. Unless otherwise noted, for all tests, nonparametric two-tailed Wilcoxon rank-sum (equivalent to Mann–Whitney *U* test), Wilcoxon signed-rank or Kruskal–Wallis one-way analysis of variance were used. Due to experimental design constraints, the experimenter was not blind to the manipulation performed during the experiment.

RESULTS

Hippocampal Temperature Correlates with Brain States

Brain temperature showed wide fluctuations (~3°C) across natural behaviors (Fig. 1, *A–C*). Waking during exercise had the highest mean temperature (36.1 ± 0.42°C, means ± SD), whereas the lowest temperature level was observed during sleep (nonREM 35.5 ± 0.44°C; REM 35.4 ± 0.42°C, means ± SD). The wake-sleep state variation was described quantitatively by the autocorrelogram of the temperature, corresponding to approximately a 90-min cycle (Fig. 1*D*). The fastest brain temperature changes occurred at the transitions between brain states. The fastest change occurred at the onset of REM sleep (Fig. 1*E*), with an average temperature increases of >0.3°C within 2 min. After nonREM onset, brain temperature decreased more gradually by > 0.1°C within a few minutes (Fig. 1*F*), whereas wake onset showed a gradual increase (Fig. 1*G*). The short transient microarousals of nonREM sleep (41) did not bring about an obvious change in temperature (Fig. 1*H*). These brain state changes were associated with characteristic changes of the θ-δ ratio (θ range: 5–12 Hz, δ range: 0–4 Hz) and movement (Fig. 1, *E–H*).

Hippocampal Ripple Metrics Correlate with Brain Temperature in Freely Moving Rats

Next, we characterized various hippocampal ripple metrics with the continuous brain temperature readings. Ripple

Table 1. *Key resources*

Resource	Source	Identifier/Location	Description
Subjects			
Rat: Long–Evans	Charles River	Cat No. Crl:LE 006	10 male adults
Data			
Hippocampal data	All authors	https://buzsakilab.com/wp/database/ (42)	Public data share with data from our lab
Software			
CellExplorer, NeuroScope2, and StateExplorer		CellExplorer.org/(40)	Cell-classification pipeline and GUI built in MATLAB
MATLAB	MathWorks	https://www.mathworks.com/	
Buzcode	Buzsaki Lab	https://github.com/buzsakilab/buzcode	MATLAB analysis tools
FMA Toolbox	Michaël Zugaro	http://fmatoolbox.sourceforge.net/	MATLAB toolbox for Freely Moving Animal (FMA)
Other			
Silicon probe (5 × 12, 6 × 10)	NeuroNexus	https://neuronexus.com/	
Silicon probe (4 × 16)	Cambridge Neurotech	https://www.cambridgeneurotech.com/	
Wire electrodes	California Fine Wire	Tungsten 99.95% (100211), insulated with Heavy Polyimide (HML - Green)	
Intan RHD2000	Intan Technologies	https://intantech.com/	
Motive tracking system	Optitrack	http://optitrack.com/	6 Flex3 camera system

frequency and the rate of SPW-R events showed large variations both across wake-sleep states as well as within nonREM and awake (Fig. 2, *A–F*). Within long sleep episodes, a positive relationship between temperature, ripple frequency, and rate of SPW-R occurrence was often visible. We observed a positive correlation between the ripple peak frequency and brain temperature (R_{nonREM} = 0.60 and R_{awake} = 0.51; n = 15 sessions). A negative correlation was observed between the ripple duration and the brain temperature (R_{nonREM} = −0.48 and R_{awake} = −0.267; n = 15 sessions). The ripple occurrence rate was correlated with brain temperature yet with larger variance between sessions (R_{nonREM} = 0.19 and R_{awake} = −0.20; n = 15 sessions). Quantification of these relationships showed a significant difference between nonREM and waking for ripple frequency and rate of SPW-Rs but not for their duration (Fig. 2, *G–I*). We also calculate the temperature correlations of these same measures, which remained unchanged between nonREM and wake brain states.

Multivariable Linear Regression Model Prediction of Ripple Frequency

To assess the potential contribution of other factors, besides temperature, in describing the ripple frequency, we applied a multivariable linear regression model, taking brain temperature, the power spectrum slope, brain states (awake, nonREM, REM, and micro arousals), SPW-R rate, and the θ-δ ratio, which are changing on a similar timescale. Using a leave-one-out approach, in which we compared the performance of a linear regression model based on all parameters versus a model in which one of the parameters were left out, we found that the brain temperature was the strongest contributor, significantly higher than the other variables as quantified by the root mean squared error (RMSE; Fig. 3*A*).

To validate that the other measures were not covariating, thus masking a potential hidden contribution to the regression model when leaving out a predictor, we also applied the same analysis using single variables. Again, the best single predictor was the brain temperature, with the lowest RMSE (Fig. 3*B*).

Local Temperature Manipulation of the Hippocampus

In a further attempt to disentangle the hypothesized temperature effect on ripples from potential hidden factors, we varied the local temperature in the hippocampus. We built a device that allowed for focal cooling and heating in freely

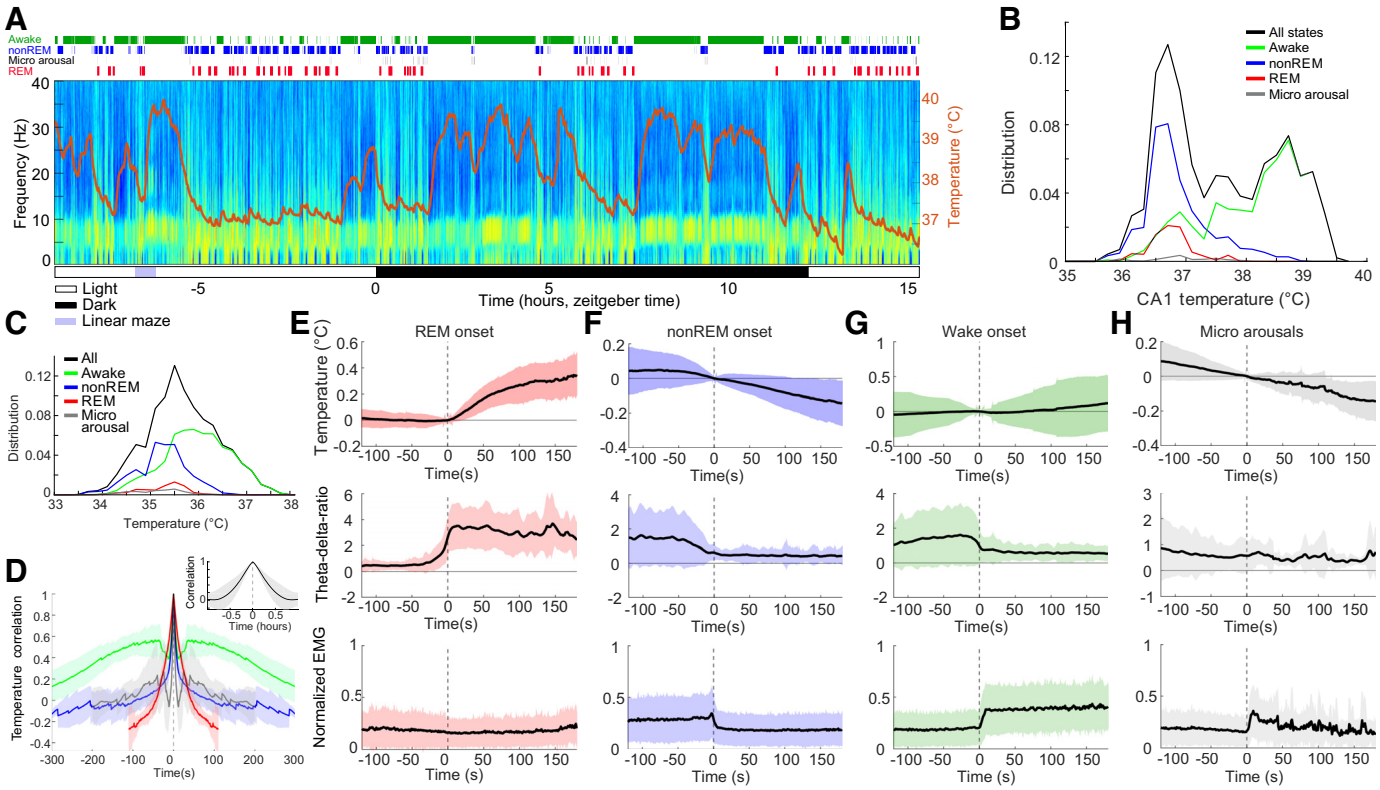

Figure 1. Hippocampal temperature varies across brain states. Twenty-four hours recording of hippocampal activity and brain temperature in a chronically implanted rat. *A*: time-power analysis of hippocampal local field potentials (LFPs) and brain temperature (orange line overlayed on spectrogram). Local field potential from the CA1 region of the hippocampus was used to calculate the time-resolved fast Fourier transform-based power spectrum. Brain state classification (41) is shown above the spectrum (awake, nonREM, micro arousals, and REM; green, blue, black, and red lines, respectively). Note steep temperature rise during maze running (purple rectangle, ∼2.5 h). *B*: brain temperature varied ∼3°C–4°C within 24 h (black), with differing distributions across brain states (awake, nonREM, micro arousals, and REM; green, blue, black, and red lines, respectively). *C*: distribution of brain temperatures across 18 recording sessions in 8 animals. *D*: 5-min wide average auto-correlograms for each brain state (same color scale as in *C*). REM sleep did not allow for more than −100-s: + 100-s window due to their short duration. *Inset*: 1 h wide temperature auto-correlogram capturing the timescale of the temperature fluctuations across states. *E*: REM onset-triggered brain temperature changes (*top*), θ-δ ratio and normalized EMG (*bottom*). *F–H*: same panels as in *E* for nonREM onset (*F*), wake onset (*G*), and micro arousals (*H*). REM, rapid eye movement.

J Neurophysiol • doi:10.1152/jn.00047.2022 • www.jn.org

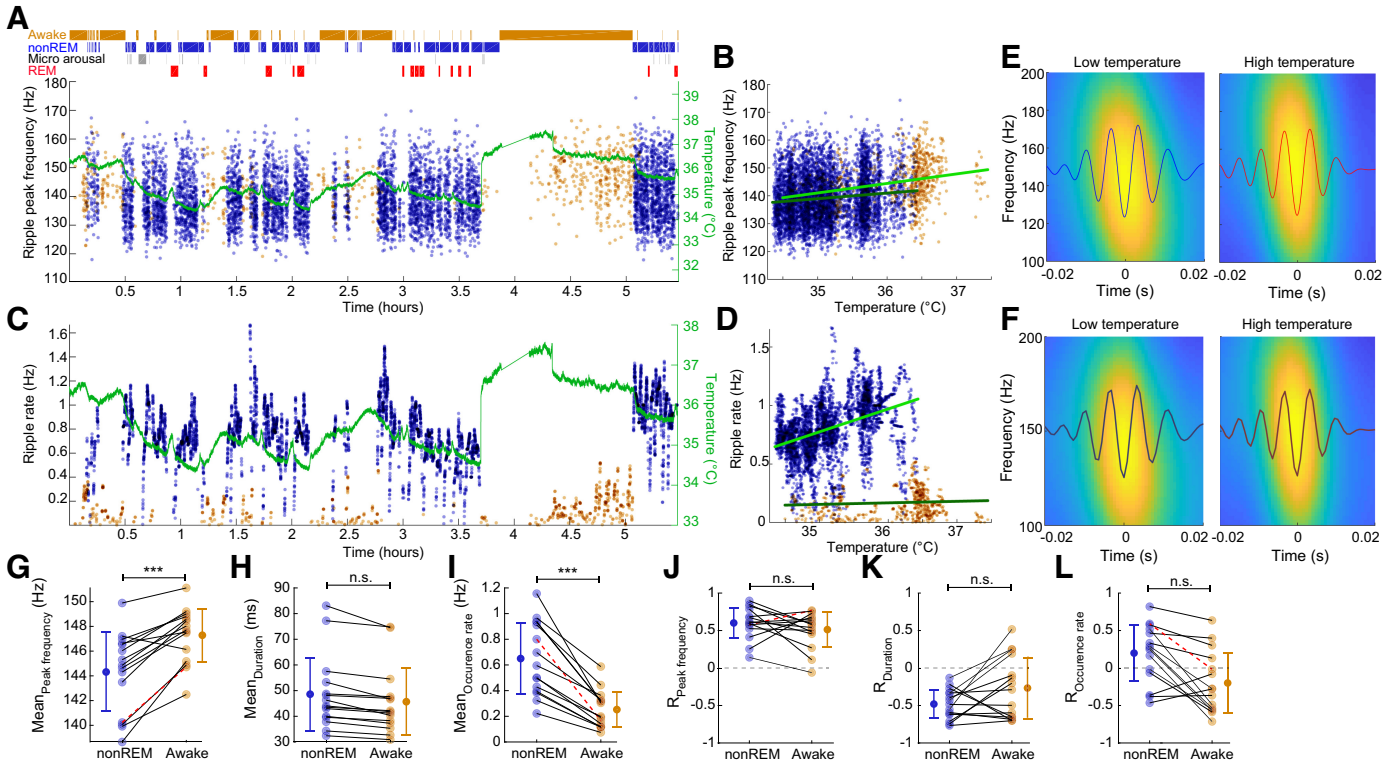

Figure 2. Hippocampal SPW-R metrics correlate with brain temperature. *A*: peak frequency of ripples (nonREM = blue dots; waking = brown dots) and brain temperature (green line) across time. *B*: correlation between temperature fluctuation and peak frequency of ripples during nonREM and waking (R_{nonREM} = 0.60, $P < 0.001$, slope = 2.01 Hz/°C; R_{wake} = 0.77, $P < 0.001$, slope = 3.41 Hz/°C; from 1 session). *C*: rate of SPW-Rs and brain temperature across time (ripple rate is calculated in 30-s intervals within brain states). Temperature line is superimposed to facilitate comparison (as in *A*). Note parallel change of SPW-R rate with temperature. Also note small but reliable temperature increase during REM episodes. *D*: correlation between temperature fluctuation and the rate of SPW-R occurrence during nonREM and waking (R_{nonREM} = 0.41, $P < 0.001$, slope = 0.20 Hz/°C; R_{awake} = 0.06, n.s., slope = 0.01 Hz/°C). *E*: average ripple waveforms and wavelet maps for low (200 ripples) and high (200 ripples) temperature epochs from the session shown *A–D*, *n* = 6673 ripples in session. *F*: average ripple waveforms and wavelet maps for low (200 ripples) and high (200 ripples) temperature epochs for all sessions. *G–I*: peak ripple frequency, mean duration, and mean rate of SPW-R occurrence during nonREM and waking. Pairs of recordings from the same session are connected. *J–L*: correlation values between brain temperature and peak ripple frequency, duration, and occurrence rate of SPW-R during nonREM and waking. Red highlighting lines in *G*, *I*, *J*, and *L* are values from the session shown in *A–E*. REM, rapid eye movement; SPW-R, sharp wave-ripple complex. ***$P < 0.001$; n.s., not significant.

moving rats (32, 35, 43). The temperature manipulation probe consists of a silver wire (260 μm in diameter), air isolation, and a polyimide tube (Fig. 4*A*). The back end of the silver wire was coiled at the cold plate of a peltier device (1.2 mm by 1.9 mm), with an added passive copper heatsink. Cooling and heating were achieved by directing current through the peltier device. A small temperature sensor (thermistor; 280 μm in diameter) was attached at the tip of the cooling probe for continuous monitoring of the local brain temperature. The cooling probe was implanted in the CA1 region together with a silicon probe 1 mm apart (Fig. 4, *A–D*). By reversing the current, we were able to induce both local heating and cooling within the same recording session (Fig. 4, *E–G*). Local temperature manipulation did not affect the sleep-wave cycle or within-sleep state changes (Supplemental Fig. S1 and S2). Local cooling (Δ_{temp} = −2.8°C) significantly lowered the ripple frequency on the ipsilateral side by ∼1.7 Hz (n = 12 sessions, P = 0.034, Wilcoxon signed rank test), whereas heating (Δ_{temp} = 3.7°C) increased ripple frequency by 1.5 Hz (Fig. 4*H*; n = 12 sessions, P = 0.012, Wilcoxon signed rank test). Ripple duration and the occurrence of ripple rates was not consistently affected by the local manipulation of the temperature (Fig. 4, *I* and *J*). Although heating increased ripple duration, cooling had no effect (Fig. 4*I*; n = 12 cooling sessions, P = 0.016; n = 12 heating sessions; P = 0.077). In contrast, cooling had no effect on SPW-R rate, whereas heating had a small, although significant increase (Fig. 4*J*; n = 12 cooling sessions, P = 0.30; n = 12 heating sessions; P = 0.027). Identical temperature manipulation of the contralateral hippocampus was without an effect (Supplemental Fig. S3; n = 5 cooling sessions, P = 0.99, n = 8 heating sessions, P = 0.52, two-sample Kolmogorov–Smirnov test).

DISCUSSION

We found a correlation between physiological brain temperature variations and the frequency of hippocampal ripples. In addition, we replicated the temperature effect by local cooling and heating the hippocampal CA1 region. The decrease and increase in ripple frequency upon cooling and heating, respectively, suggest that brain temperature is the main mechanism responsible for the ripple frequency differences between sleeping and waking animals. In contrast to changes in ripple frequency, the rate of occurrence of SPW-Rs and ripple duration were only marginally affected by local

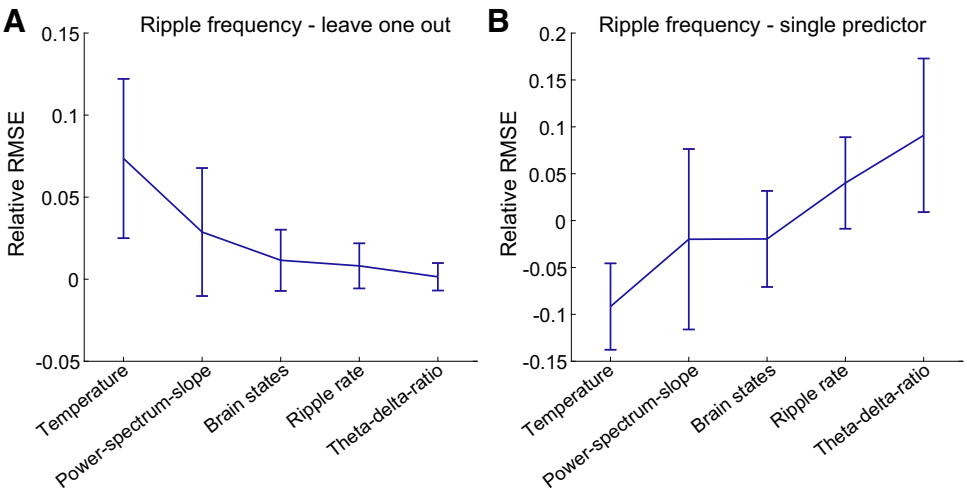

Figure 3. The brain temperature is the best predictor of ripple frequency. *A*: leave-one-out prediction of ripple frequency dynamics. Root mean squared error (RMSE) difference for each held-out predictor. The held-out predictor is labeled along the *x*-axis. *B*: same analysis as in *A* but using only one predictor at the time, showing the lowest error when predicting the ripple frequency via brain temperature (ANOVA paired test $P < 0.005$ for all pairs). Predictors: Brain temperature, power-spectrum-slope, brain states (awake, nonREM, or REM), ripple rate, θ-δ ratio. REM, rapid eye movement.

temperature perturbation, suggesting that the control mechanisms of these parameters reside upstream from the CA1 region.

The effect of ambient temperature on the nervous system and behavior is strong in cold-blooded animals (34). In homoiotherm birds and mammals, although body and brain temperature are homeostatically regulated, there is still a systematic and consistent variation in brain temperature, corresponding to ~3°C in birds, rodents, and humans (32, 44, 45) and even much larger changes are present in hibernating animals (46). During sustained nonREM sleep, temperature on the neocortical surface of mice decreases by ~2°C (47), and recent work indicates that a specific hypothalamic circuitry exists to deliberately cool the brain and simultaneously induce nonREM sleep (48, 49). Our findings confirm previous observations in the rodent regarding the behavior and brain-state dependence of temperature variation (30, 33, 50, 51).

We extend these previous findings by quantifying the relationship between brain temperature and both SPW-R occurrence, duration, and ripple frequency. The hippocampal SPW-R is a complex pattern of two independent but coupled events. The extracellular sharp wave (SPW) is produced by large transmembrane currents in the apical dendrites of CA1 pyramidal cell, which are triggered by the synchronous CA3 input targeting the mid stratum radiatum (20). The CA3 volley also excites CA1 interneurons to protract the rate of pyramidal neuron recruitment and their interaction induces a short-lived fast oscillation (110–160 Hz) detected in the local field potential (LFP) as a "ripple" (4, 21–23). The two mechanisms can be dissociated by separate perturbations of the CA1 and CA3 regions (52–54). In our experiments, physiological decrease of brain temperature during nonREM sleep was correlated with both the rate of SPW-Rs and ripple frequency, presumably because both the CA1 region and regions upstream to it were cooled. In contrast, artificial manipulation of local CA1 temperature affected ripple frequency but had an inconsistent effect on SPW-R rate. We assume that the minor change of SPW-R rate with temperature increase was due to increasing the temperature also in the CA3 region. This is consistent with previous observations that although the spatial temperature gradient is steep, nevertheless it can have a detectable effect a few millimeters from the probe (32, 35). The same manipulation of the contralateral CA1 region was without an effect, further supporting the role of local CA1 mechanisms for controlling ripple frequency (22). The difference between ripple frequency in the waking and sleeping rat was ~5 Hz (9). In contrast, perturbation of local CA1 temperature brought about only 2–4 Hz shifts. Thus, one may suggest that other factors than cooling play an important role in decreasing ripple frequency during nonREM sleep. However, axons of fast firing CA1 basket cells, the presumed substrate of ripple frequency generation (22, 55), reach the entire fimbio-subicular extent of CA1 and up to 1 mm along the long axis (56). Thus, many cell bodies of basket cells residing outside the effectively cooled local patch could have counteracted the frequency decrease brought about by the locally cooled neurons. The primacy of temperature control of ripple frequency is further supported by our statistical analyses, which showed that the best single predictor of ripple frequency was temperature, rather than power spectrum slope, brain state, global firing rate, or θ-δ ratio of LFP.

How does temperature affect ripple frequency? The key determinant of ripple frequency is the fast-reacting $GABA_A$ receptors on the dendrites of basket cells (22). Previous work in vitro has demonstrated that cooling the brain slice by only 2°, the time constant of inhibitory postsynaptic currents in the hippocampus increased by about the same extent as induced by $GABA_A$ receptor blockers and general anesthetics at sedative doses (57). Conversely, drugs affecting brain temperature may exert an effect on circuit operations and behavior mediated by direct temperature changes. Auxiliary mechanisms could involve the expression of the cold-inducible RNA-binding protein (CIRBP) and RNA-binding motif protein 3 genes (58). However, the proteins encoded by these genes are likely required for structural remodeling and their involvement in the fast communication among interneurons has yet to be uncovered. In summary, the physiological changes of brain temperature between waking and nonREM sleep appears to be the major mechanism for altering the frequency of hippocampal ripples.

DATA AVAILABILITY

The dataset is publicly available from our data bank (42) via our website: https://buzsakilab.com/wp/projects/entry/66407/.

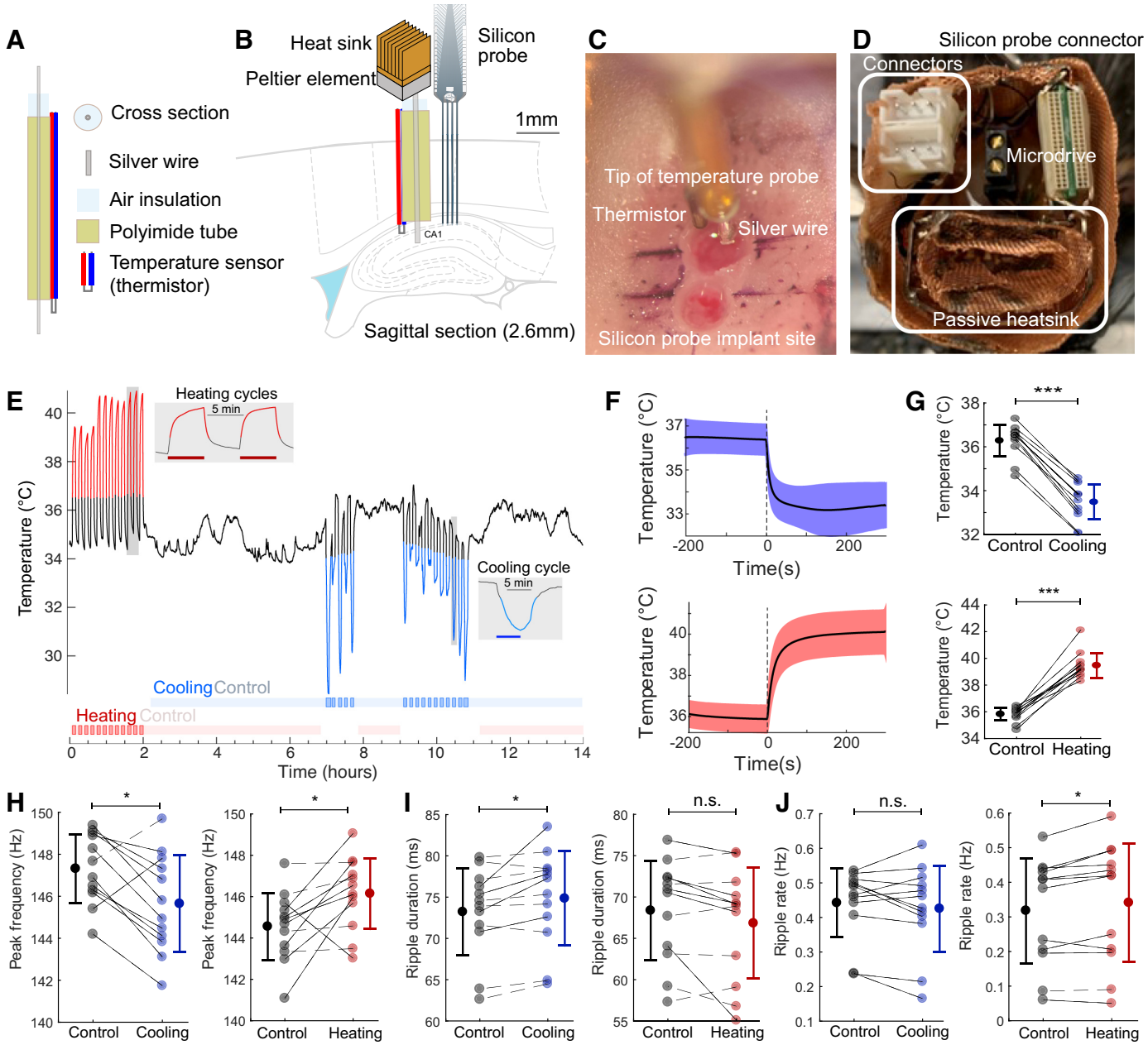

Figure 4. Local temperature manipulation affects ripple frequency. *A* and *B*: cooling probe and silicon probe or tungsten wires were implanted in the CA1 region of the hippocampus of rats. Peltier element with heatsink is coupled to the silver wire and the hippocampus is cooled by thermal conduction. *C*: intraoperative photograph showing the implanted cooling device (*top*) and the location of the probe implantation (*bottom*). Black marker lines are approximately 1 mm apart. *D*: additional copper mesh heatsink is attached to the peltier element and placed inside the on-head Faraday cage. Custom connectors (for peltier probe and thermistor) are highlighted on the *left*. Omnetics connector of the silicon probe and microdrive in black are also shown. *E*: CA1 temperature during local temperature manipulation. Cooling intervals are shown by a blue line, and heating intervals by red line. Manipulation intervals were defined using the graphical interface StateExplorer (Supplemental Fig. S1). Red/blue horizontal bars in *insets* are the true 5 min heating/cooling intervals applied with the peltier device. *F*: time course of local temperature change during cooling and heating. *G*: temperature changes during individual cooling and heating sessions (cooling: $P = 0.0005$, Wilcoxon signed rank test, $n = 12$ sessions in 3 rats and heating: $P = 0.0005$, Wilcoxon signed rank test, $n = 12$ sessions in 4 rats). *H*: peak frequency of ripples during cooling (*left*; $\Delta_{freq} = -1.7$ Hz, $P = 0.034$) and heating sessions (*right*; $\Delta_{freq} = 1.5$ Hz, $P = 0.012$). Solid lines represent sessions with significant within-session modulation ($P < 0.01$, Kolmogorov–Smirnov test), and dashed lines represent sessions with nonsignificant modulation ($P > 0.05$, Kolmogorov–Smirnov test). *I*: ripple duration (cooling: $\Delta_{duration} = 1.6$ ms, $P = 0.016$; heating: $\Delta_{duration} = -1.6$ ms, $P = 0.077$). *J*: rate of ripple occurrence (cooling: $\Delta_{rate} = -0.012$ Hz, $P = 0.30$; heating: $\Delta_{rate} = 0.02$ Hz, $P = 0.027$; same sessions shown in *G*–*J*; Wilcoxon signed rank test applied in all stats). $^*P < 0.05$, $^{***}P < 0.001$; n.s., not significant.

SUPPLEMENTAL DATA

Supplemental Figs. S1–S3 and Supplemental Table S1 are available at https://doi.org/10.6084/m9.figshare.19146287.

GRANTS

This work was supported by the National Institutes of Health (NIH) Grants U19 NS107616 and R01MH122391, the Independent Research Fund Denmark, and Lundbeckfonden Denmark.

DISCLOSURES

No conflicts of interest, financial or otherwise, are declared by the authors.

AUTHOR CONTRIBUTIONS

P.C.P., M.V., and G.B. conceived and designed research; M.V. and P.C.P. performed experiments; P.P. analyzed data; P.C.P., M.V., and G.B. interpreted results of experiments; P.C.P. and M.V. prepared figures; G.B., P.C.P., and M.V. drafted manuscript; G.B., P.C.P., and M.V. edited and revised manuscript; P.C.P., M.V., and G.B. approved final version of manuscript.

ENDNOTE

At the request of the authors, readers are herein alerted to the fact that additional materials related to this manuscript may be found at https://buzsakilab.com/wp/projects/entry/66407/. These materials are not a part of this manuscript and have not undergone peer review by the American Physiological Society (APS). APS and the journal editors take no responsibility for these materials, for the website address, or for any links to or from it.

REFERENCES

1. **Maguire EA**, **Hassabis D.** Role of the hippocampus in imagination and future thinking. *Proc Natl Acad Sci USA* 108: E39–E39, 2011. doi:10.1073/pnas.1018876108.
2. **Schacter DL**, **Addis DR**, **Buckner RL.** Remembering the past to imagine the future: the prospective brain. *Nat Rev Neurosci* 8: 657–661, 2007. doi:10.1038/nrn2213.
3. **Vanderwolf CH.** Hippocampal electrical activity and voluntary movement in the rat. *Electroencephalogr Clin Neurophysiol* 26: 407–418, 1969. doi:10.1016/0013-4694(69)90092-3.
4. **Buzsáki G**, **Horváth Z**, **Urioste R**, **Hetke J**, **Wise K.** High-frequency network oscillation in the hippocampus. *Science* 256: 1025–1027, 1992. doi:10.1126/science.1589772.
5. **Girardeau G**, **Benchenane K**, **Wiener SI**, **Buzsáki G**, **Zugaro MB.** Selective suppression of hippocampal ripples impairs spatial memory. *Nat Neurosci* 12: 1222–1223, 2009. doi:10.1038/nn.2384.
6. **Miyawaki H**, **Diba K.** Regulation of hippocampal firing by network oscillations during sleep. *Curr Biol* 26: 893–902, 2016. doi:10.1016/j.cub.2016.02.024.
7. **Norimoto H**, **Makino K**, **Gao M**, **Shikano Y**, **Okamoto K**, **Ishikawa T**, **Sasaki T**, **Hioki H**, **Fujisawa S**, **Ikegaya Y.** Hippocampal ripples down-regulate synapses. *Science* 359: 1524–1527, 2018. doi:10.1126/science.aao0702.
8. **Tingley D**, **McClain K**, **Kaya E**, **Carpenter J**, **Buzsáki G.** A metabolic function of the hippocampal sharp wave-ripple. *Nature* 597: 82–86, 2021. doi:10.1038/s41586-021-03811-w.
9. **Roumis DK**, **Frank LM.** Hippocampal sharp-wave ripples in waking and sleeping states. *Curr Opin Neurobiol* 35: 6–12, 2015. doi:10.1016/j.conb.2015.05.001.
10. **Diba K**, **Buzsáki G.** Forward and reverse hippocampal place-cell sequences during ripples. *Nat Neurosci* 10: 1241–1242, 2007. doi:10.1038/nn1961.
11. **Nádasdy Z**, **Hirase H**, **Czurkó A**, **Csicsvari J**, **Buzsáki G.** Replay and time compression of recurring spike sequences in the hippocampus. *J Neurosci* 19: 9497–9507, 1999. doi:10.1523/JNEUROSCI.19-21-09497.1999.
12. **Pfeiffer BE**, **Foster DJ.** Hippocampal place-cell sequences depict future paths to remembered goals. *Nature* 497: 74–79, 2013. doi:10.1038/nature12112.
13. **Wilson MA**, **McNaughton BL.** Reactivation of hippocampal ensemble memories during sleep. *Science* 265: 676–679, 1994. doi:10.1126/science.8036517.
14. **Gillespie AK**, **Astudillo Maya DA**, **Denovellis EL**, **Liu DF**, **Kastner DB**, **Coulter ME**, **Roumis DK**, **Eden UT**, **Frank LM.** Hippocampal replay reflects specific past experiences rather than a plan for subsequent choice. *Neuron* 109: 3149–3163.e6, 2021. doi:10.1016/j.neuron.2021.07.029.
15. **Roux L**, **Hu B**, **Eichler R**, **Stark E**, **Buzsáki G.** Sharp wave ripples during learning stabilize the hippocampal spatial map. *Nat Neurosci* 20: 845–853, 2017. doi:10.1038/nn.4543.
16. **Dupret D**, **O'Neill J**, **Pleydell-Bouverie B**, **Csicsvari J.** The reorganization and reactivation of hippocampal maps predict spatial memory performance. *Nat Neurosci* 13: 995–1002, 2010. doi:10.1038/nn.2599.
17. **Joo HR**, **Frank LM.** The hippocampal sharp wave–ripple in memory retrieval for immediate use and consolidation. *Nat Rev Neurosci* 19: 744–757, 2018. doi:10.1038/s41583-018-0077-1.
18. **Ólafsdóttir HF**, **Bush D**, **Barry C.** The role of hippocampal replay in memory and planning. *Curr Biol* 28: R37–R50, 2018. doi:10.1016/j.cub.2017.10.073.
19. **Buzsáki G.** Two-stage model of memory trace formation: a role for "noisy" brain states. *Neuroscience* 31: 551–570, 1989. doi:10.1016/0306-4522(89)90423-5.
20. **Buzsáki G**, **Leung LW**, **Vanderwolf CH.** Cellular bases of hippocampal EEG in the behaving rat. *Brain Res* 6: 139–171, 1983. doi:10.1016/0165-0173(83)90037-1.
21. **O'Keefe J**, **Nadel L.** *The Hippocampus as a Cognitive Map*. Oxford, UK: Clarendon Press, 1978.
22. **Stark E**, **Roux L**, **Eichler R**, **Senzai Y**, **Royer S**, **Buzsáki G.** Pyramidal cell-interneuron interactions underlie hippocampal ripple oscillations. *Neuron* 83: 467–480, 2014. doi:10.1016/j.neuron.2014.06.023.
23. **Ylinen A**, **Soltész I**, **Bragin A**, **Penttonen M**, **Sik A**, **Buzsáki G.** Intracellular correlates of hippocampal theta rhythm in identified pyramidal cells, granule cells, and basket cells. *Hippocampus* 5: 78–90, 1995. doi:10.1002/hipo.450050110.
24. **Schomburg EW**, **Anastassiou CA**, **Buzsáki G**, **Koch C.** The spiking component of oscillatory extracellular potentials in the rat hippocampus. *J Neurosci* 32: 11798–11811, 2012. doi:10.1523/JNEUROSCI.0656-12.2012.
25. **Dijk DJ**, **Czeisler CA.** Contribution of the circadian pacemaker and the sleep homeostat to sleep propensity, sleep structure, electroencephalographic slow waves, and sleep spindle activity in humans. *J Neurosci* 15: 3526–3538, 1995. doi:10.1523/JNEUROSCI.15-05-03526.1995.
26. **Franks NP**, **Wisden W.** The inescapable drive to sleep: overlapping mechanisms of sleep and sedation. *Science* 374: 556–559, 2021. doi:10.1126/science.abi8372.
27. **Andersen P**, **Moser EI.** Brain temperature and hippocampal function. *Hippocampus* 5: 491–498, 1995. doi:10.1002/hipo.450050602.
28. **Csernai M**, **Borbély S**, **Kocsis K**, **Burka D**, **Fekete Z**, **Balogh V**, **Káli S**, **Emri Z**, **Barthó P.** Dynamics of sleep oscillations is coupled to brain temperature on multiple scales. *J Physiol* 597: 4069–4086, 2019. doi:10.1113/JP277664.
29. **Deboer T.** Brain temperature dependent changes in the electroencephalogram power spectrum of humans and animals. *J Sleep Res* 7: 254–262, 1998. doi:10.1046/j.1365-2869.1998.00125.x.
30. **Franken P**, **Tobler I**, **Borbély AA.** Sleep and waking have a major effect on the 24-hr rhythm of cortical temperature in the rat. *J Biol Rhythms* 7: 341–352, 1992. doi:10.1177/074873049200700407.
31. **Hubbard J**, **Gent TC**, **Hoekstra MMB**, **Emmenegger Y**, **Mongrain V**, **Landolt H-P**, **Adamantidis AR**, **Franken P.** Rapid fast-delta decay following prolonged wakefulness marks a phase of wake-inertia in NREM sleep. *Nat Commun* 11: 3130, 2020. doi:10.1038/s41467-020-16915-0.
32. **Long MA**, **Fee MS.** Using temperature to analyse temporal dynamics in the songbird motor pathway. *Nature* 456: 189–194, 2008. doi:10.1038/nature07448.

33. **Moser E**, **Mathiesen I**, **Andersen P.** Association between brain temperature and dentate field potentials in exploring and swimming rats. *Science* 259: 1324–1326, 1993. doi:10.1126/science.8446900.
34. **O'Leary T**, **Marder E.** Temperature-robust neural function from activity-dependent ion channel regulation. *Curr Biol* 26: 2935–2941, 2016. doi:10.1016/j.cub.2016.08.061.
35. **Petersen PC**, **Buzsáki G.** Cooling of medial septum reveals theta phase lag coordination of hippocampal cell assemblies. *Neuron* 107: 731–744.e3, 2020. doi:10.1016/j.neuron.2020.05.023.
36. **Sheroziya M**, **Timofeev I.** Moderate cortical cooling eliminates thalamocortical silent states during slow oscillation. *J Neurosci* 35: 13006–13019, 2015. doi:10.1523/JNEUROSCI.1359-15.2015.
37. **McGinty D**, **Szymusiak R.** Keeping cool: a hypothesis about the mechanisms and functions of slow-wave sleep. *Trends Neurosci* 13: 480–487, 1990. doi:10.1016/0166-2236(90)90081-K.
38. **Vöröslakos M**, **Miyawaki H**, **Royer S**, **Diba K**, **Yoon E**, **Petersen PC**, **Buzsáki G.** 3D-printed recoverable microdrive and base plate system for rodent electrophysiology. *Bio Protoc* 11: e4137, 2021. doi:10.21769/BioProtoc.4137.
39. **Mizuseki K**, **Diba K**, **Pastalkova E**, **Buzsáki G.** Hippocampal CA1 pyramidal cells form functionally distinct sublayers. *Nat Neurosci* 14: 1174–1181, 2011. doi:10.1038/nn.2894.
40. **Petersen PC**, **Siegle JH**, **Steinmetz NA**, **Mahallati S**, **Buzsáki G.** CellExplorer: a framework for visualizing and characterizing single neurons. *Neuron* 109: 3594–3608.e2, 2021. doi:10.1016/j.neuron.2021.09.002.
41. **Watson BO**, **Levenstein D**, **Greene JP**, **Gelinas JN**, **Buzsáki G.** Network homeostasis and state dynamics of neocortical sleep. *Neuron* 90: 839–852, 2016. doi:10.1016/j.neuron.2016.03.036.
42. **Petersen PC**, **Hernandez M**, **Buzsáki G.** The Buzsaki Lab Databank - Public electrophysiological datasets from awake animals. *Zenodo*, 2020. doi:10.5281/zenodo.4307883.
43. **Aronov D**, **Fee MS.** Analyzing the dynamics of brain circuits with temperature: design and implementation of a miniature thermoelectric device. *J Neurosci Methods* 197: 32–47, 2011. doi:10.1016/j.jneumeth.2011.01.024.
44. **Moser EI**, **Andersen P.** Conserved spatial learning in cooled rats in spite of slowing of dentate field potentials. *J Neurosci* 14: 4458–4466, 1994. doi:10.1523/JNEUROSCI.14-07-04458.1994.
45. **Kiyatkin EA**, **Brown PL**, **Wise RA.** Brain temperature fluctuation: a reflection of functional neural activation. *Eur J Neurosci* 16: 164–168, 2022. doi:10.1046/j.1460-9568.2002.02066.x.
46. **Ruf T**, **Geiser F.** Daily torpor and hibernation in birds and mammals. *Biol Rev Camb Philos Soc* 90: 891–926, 2015. doi:10.1111/brv.12137.
47. **Fuller A**, **Carter RN**, **Mitchell D.** Brain and abdominal temperatures at fatigue in rats exercising in the heat. *J Appl Physiol (1985)* 84: 877–883, 1998. doi:10.1152/jappl.1998.84.3.877.
48. **Harding EC**, **Franks NP**, **Wisden W.** Sleep and thermoregulation. *Curr Opin Physiol* 15: 7–13, 2020. doi:10.1016/j.cophys.2019.11.008.
49. **Harding EC**, **Ba W**, **Zahir R**, **Yu X**, **Yustos R**, **Hsieh B**, **Lignos L**, **Vyssotski AL**, **Merkle FT**, **Constandinou TG**, **Franks NP**, **Wisden W.** Nitric oxide synthase neurons in the preoptic hypothalamus are NREM and REM sleep-active and lower body temperature. *Front Neurosci* 15: 709825, 2021. doi:10.3389/fnins.2021.709825.
50. **Alföldi P**, **Tobler I**, **Borbély AA.** Sleep regulation in rats during early development. *Am J Physiol Regul Integr Comp Physiol* 258: R634–R644, 1990. doi:10.1152/ajpregu.1990.258.3.R634.
51. **Hayward J**, **Baker M.** Role of cerebral arterial blood in the regulation of brain temperature in the monkey. *Am J Physiol* 215: 389–403, 1968. doi:10.1152/ajplegacy.1968.215.2.389.
52. **Davoudi H**, **Foster DJ.** Acute silencing of hippocampal CA3 reveals a dominant role in place field responses. *Nat Neurosci* 22: 337–342, 2019. doi:10.1038/s41593-018-0321-z.
53. **Nakazawa K**, **Quirk MC**, **Chitwood RA**, **Watanabe M**, **Yeckel MF**, **Sun LD**, **Kato A**, **Carr CA**, **Johnston D**, **Wilson MA**, **Tonegawa S.** Requirement for hippocampal CA3 NMDA receptors in associative memory recall. *Science* 297: 211–218, 2002. doi:10.1126/science.1071795.
54. **Rogers S**, **Rozman PA**, **Valero M**, **Doyle WK**, **Buzsáki G.** Mechanisms and plasticity of chemogenically induced interneuronal suppression of principal cells. *Proc Natl Acad Sci USA* 118: e2014157118, 2021. doi:10.1073/pnas.2014157118.
55. **Chiovini B**, **Turi GF**, **Katona G**, **Kaszás A**, **Pálfi D**, **Maák P**, **Szalay G**, **Szabó MF**, **Szabó G**, **Szadai Z**, **Káli S**, **Rózsa B.** Dendritic spikes induce ripples in parvalbumin interneurons during hippocampal sharp waves. *Neuron* 82: 908–924, 2014 [Erratum in *Neuron* 83: 749, 2014]. doi:10.1016/j.neuron.2014.04.004.
56. **Sik A**, **Penttonen M**, **Ylinen A**, **Buzsaki G.** Hippocampal CA1 interneurons: an in vivo intracellular labeling study. *J Neurosci* 15: 6651–6665, 1995. doi:10.1523/JNEUROSCI.15-10-06651.1995.
57. **Franks NP.** General anaesthesia: from molecular targets to neuronal pathways of sleep and arousal. *Nat Rev Neurosci* 9: 370–386, 2008. doi:10.1038/nrn2372.
58. **Morf J**, **Rey G**, **Schneider K**, **Stratmann M**, **Fujita J**, **Naef F**, **Schibler U.** Cold-inducible RNA-binding protein modulates circadian gene expression posttranscriptionally. *Science* 338: 379–383, 2012. doi:10.1126/science.1217726.